Journal of Systems Engineering and Electronics
Vol. 35, No. 1, February 2024, pp.242 – 258

Robust design of sliding mode control for airship trajectory tracking with uncertainty and disturbance estimation

WASIM Muhammad[1,*], ALI Ahsan[2], CHOUDHRY Mohammad Ahmad[2], SHAIKH Inam Ul Hasan[1], and SALEEM Faisal[3,4]

1. Department of Aeronautics and Astronautics Engineering, Institute of Space Technology, Islamabad 44000, Pakistan;
2. Department of Electrical Engineering, University of Engineering and Technology, Taxila 47080, Pakistan;
3. Department of Measurements and Control Systems, Silesian University of Technology, Gliwice 44-101, Poland;
4. The Joint Doctoral School, Silesian University of Technology, Gliwice 44-100, Poland

Abstract: The robotic airship can provide a promising aerostatic platform for many potential applications. These applications require a precise autonomous trajectory tracking control for airship. Airship has a nonlinear and uncertain dynamics. It is prone to wind disturbances that offer a challenge for a trajectory tracking control design. This paper addresses the airship trajectory tracking problem having time varying reference path. A lumped parameter estimation approach under model uncertainties and wind disturbances is opted against distributed parameters. It uses extended Kalman filter (EKF) for uncertainty and disturbance estimation. The estimated parameters are used by sliding mode controller (SMC) for ultimate control of airship trajectory tracking. This comprehensive algorithm, EKF based SMC (ESMC), is used as a robust solution to track airship trajectory. The proposed estimator provides the estimates of wind disturbances as well as model uncertainty due to the mass matrix variations and aerodynamic model inaccuracies. The stability and convergence of the proposed method are investigated using the Lyapunov stability analysis. The simulation results show that the proposed method efficiently tracks the desired trajectory. The method solves the stability, convergence, and chattering problem of SMC under model uncertainties and wind disturbances.

Keywords: airship, chattering, extended Kalman filter (EKF), model uncertainties estimation, sliding mode controller (SMC).

DOI: 10.23919/JSEE.2024.000017

1. Introduction

Unmanned aerial vehicles (UAVs) are the focus of interest for researchers and developers around the world due to their enormous applications in the military, agriculture, and commercial sectors. UAVs cover a larger variety of aerial vehicles including fixed wing aircraft, quadrotors, and airships. Among them, airships are the typical type of lighter than air vehicles that take its most of lift from aerostatic forces. An airship has a prominent future due to their unique properties and their suitability for many potential applications. It can be used as an observation platform for forest monitoring. Airship can be utilized as a platform for military surveillance as well as scientific monitoring. Because an airship uses the minimum power to stay aloft, it can be operated for a prolonged period as a data collection platform [1].

They may provide a platform for agriculture monitoring equipment at low altitudes for pests, weeds, and crop data collection [2]. These applications require autonomous missions that include trajectory tracking, and path following. In trajectory tracking, an airship is required to follow a predefined path in a specific time. In path following, an airship is required to follow a certain predefined path without any time constraints. For the successful execution of the autonomous missions, it is required to develop an efficient and reliable control and navigation system for an airship. An airship trajectory tracking control design is a bit difficult due to its slow and highly coupled nonlinear dynamics. The difficulty level further increases due to its lighter than air nature because it is severely affected by wind disturbances. Model uncertainties are related to mass matrix variation in an airship model. Unknown aerodynamic model parameters also affect an airship controller performance in a similar way. Many contributions can be found in literature that discuss different control methods for airship trajectory tracking.

Linear control methods use the system linearized model and systematic rules for the design and analysis of the control system. In linear control methods, proportional-integral-derivative (PID) controller is designed for

Manuscript received December 28, 2021.
*Corresponding author.

an airship trajectory tracking [3]. Chen et al. designed a composite control scheme for airship trajectory tracking that consists of PID and dynamic inversion controller for improved performance [4]. However, the PID controller cannot ensure control capability for different operating conditions. Moutinho et al. linearized the AURORA airship model, and separated its longitudinal and lateral dynamics; based on this reduced model, a dynamic inversion controller is implemented [5]. However, this control method does not apply to all operating points due to neglecting the dynamic nonlinearities and coupling between longitudinal and lateral dynamics.

Apart from linear control methods, researchers have used model predictive control (MPC) and optimal controllers with a linear model for airship planar trajectory tracking and control of ground vehicles [6–9]. However, in [6] no mechanism for evaluating the controller under the stratospheric environment was mentioned. Too much dependence on operating space affects the performance of linear MPC. A nonlinear MPC is designed for airship spatial trajectory tracking while handling operating space limitations. Model predictive controllers solve an optimization problem on each sampling instant. The complexity of the algorithm increases with each additional state that makes it computationally intensive and restrains its use in real-time scenarios [10]. Due to these limitations, other nonlinear controllers are used for the airship trajectory tracking. Gain scheduling controller, backstepping controller, and sliding mode controller (SMC) are commonly employed to address these limitations. Gain scheduling technique was used for complete flight envelope under the project autonomous unmanned remote monitoring robotic airship (AURORA) [11]. In gain scheduling control methodology, the system model is linearized for different operating points. The controller is synthesized for each vertex and interpolation is used for the intermediate points between vertexes. The complexity of the controller synthesis increases with the number of operating points hence in certain cases the controller becomes infeasible. Therefore, many researchers have preferred other nonlinear control approaches for airship trajectory tracking.

A command filtered vectoral backstepping controller is designed for a stratospheric airship to track the three-dimensional (3D) trajectory. The command filter is used to smooth controller input derivatives for the backstepping approach employed to reduce the tracking error. The conventional backstepping method achieves robustness through high controller gain. Although the high controller gain ensures the robust performance of the controller; however, deteriorates the nominal performance [12,13]. In such cases, model deficiencies are handled through an adaptive and neural network based adaptive backstepping controllers [14–16]. Researchers have reported that the performance of the adaptive backstepping algorithm strictly depends on the initial bias and disturbance. If the initial bias and disturbance are large, the method may go unstable [17]. The use of a backstepping controller is problematic because of an "explosion of terms" in its control law, which depends on the size of the system.

SMC is designed for airship planar trajectory tracking under the project AURORA using linear longitudinal and lateral models. Longitudinal model is used for maintaining certain height of the airship and lateral model is incorporated for reducing tracking error. As model used for the controller design is linearized for airspeed of 2 ms^{-1}, so global behavior may not be guaranteed. Also, the discontinuous nature of SMC as well as the imperfections in the physical system induces high-frequency oscillations in control input called chattering. In airship control, chattering might cause damage to actuators and airships body. Attenuating the chattering is the emphasis in sliding mode control. Also, the reaching phase of the controller is sensitive to the model uncertainties and external disturbances. It degrades the performance of the controller. In certain cases, it may cause a stability problem for the system.

An airship model is usually affected by mass matrix variations, aerodynamic coefficients uncertainties, and wind disturbances. To handle the model uncertainties and external disturbances, the SMC method is applied with modifications for airship trajectory tracking. In these modified methods, usually neural network (NN), fuzzy logic (FL), and adaptive methods are utilized for the approximation of model uncertainties and external disturbances [18–26].

Adaptive SMC is designed for airship trajectory tracking where the adaptive term is used to approximate the model uncertainties. An adaptive law is also designed to tune the SMC gains to solve the chattering issue and to ensure the robustness. Apart from that, fuzzy logic and neural networks-based SMC methods are also applied for airship trajectory tracking where these terms are used to estimate the model uncertainties as well as wind disturbances. The existing literature for airship trajectory tracking control based on adaptive or intelligent methods to handle the model uncertainties and wind disturbances offers good convergence properties. However, they rely on accurate state information. While in practice states may be affected by sensor noise, sensor bias as well as the state information can be unavailable in the case of sensor failure. Also, the authenticity, comprehensiveness, and reliability of the data used for NN training are cru-

cial. In case all the scenarios of the workspace are not covered in training data then it will not perform for the missing scenarios. The data for the missing scenario need to be estimated by using some estimator.

In order to avoid computationally intensiveness and limitations of existing nonlinear control methods, extended Kalman filter (EKF) based SMC (ESMC) method is proposed for efficient and reliable trajectory tracking of a robotic airship. In the proposed work, a lumped approach as suggested in our previous work [27] for the unified estimation of deficiencies of the airship model, parameter variation, wind disturbances, and airship states using Kalman filter algorithm is used here with SMC for airship trajectory tracking. The proposed estimation method provides the combined estimate of airship states, change in the model due to mass matrix parameter variation, aerodynamic model deficiencies, and wind disturbance. The closed-loop stability and convergence of the proposed method are proved by using the Lyapunov theorem. The effectiveness of the proposed method is demonstrated through extensive numerical simulations where controller performance is evaluated under three different cases. In the first case, airship mass matrix parameters are varied. In the second case, aerodynamic model parameters are changed during airship flight. In the third case wind disturbance is considered. The results indicate that the ESMC method is not only robust against model uncertainties, but also alleviates the chattering issue and ensures good performance. The comparative simulations against SMC verify the advantages of the ESMC method.

The rest of the paper is organized as follows: In Section 2, airship nonlinear 6-DOF model is presented, and suitable assumptions are made for the incorporation of model uncertainties. In Section 3, the trajectory tracking problem is formulated, modelling of model uncertainty using a lumped approach is introduced, SMC design, ESMC design, EKF design, and EKF convergence are discussed. Section 4 discusses the simulation results where three different cases are considered for the rigorous performance evaluation of the ESMC method. Section 5 gives some concluding remarks.

2. Airship 6-DOF nonlinear model

Fig. 1 shows an airship having an ellipsoidal envelope. It is filled with low-density gas such as helium. An airship has a gondola under the envelope that carries autonomous flight control equipment, batteries, and the payload. It has two propellers on both sides of the gondola to provide the necessary thrust for an airship motion. Airship has two rudders and two elevators in the plus configuration on the tail. They provide the aerodynamic control force necessary for an airship maneuvering in cruise flight. A propeller at the bottom rudder of an airship enhances the yaw control. The introduction of two reference frames enables us to develop airship nonlinear modelling equations. The inertial frame is located at a fixed point on the earth. The local reference frame inflicts at the center of volume (CV) of an airship [28].

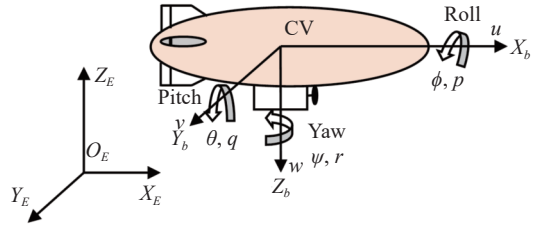

Fig. 1 Coordinate system of an airship

Airship position and attitude are expressed with respect to the inertial frame and represented by $\boldsymbol{X}=[x,y,z]$ and $\boldsymbol{\Theta}=[\phi,\theta,\psi]$, respectively. Airship linear and angular velocities aligned with local reference frame have a representation of $\boldsymbol{\upsilon}=[u,v,w]$ and $\boldsymbol{\Omega}=[p,q,r]$, respectively. Let $\boldsymbol{x}_1$ be the state vector representing the airship position and attitude. $\boldsymbol{x}_2$ is a state vector representing airship linear and angular velocities. Then the nonlinear state-space representation of an airship model can be expressed as

$$\begin{cases}\dot{\boldsymbol{x}}_1=\boldsymbol{R}(\boldsymbol{\Theta})\boldsymbol{x}_2\\ \dot{\boldsymbol{x}}_2=\bar{\boldsymbol{M}}^{-1}(\bar{\boldsymbol{F}}_{\boldsymbol{D}}+\bar{\boldsymbol{F}}_{\mathrm{AS}}+\bar{\boldsymbol{F}}_{\mathrm{AD}}+\boldsymbol{B}_{\boldsymbol{W}}+\boldsymbol{U})\end{cases}\tag{1}$$

where $\boldsymbol{x}_1\in\mathbf{R}^{6\times1}=[x,y,z,\phi,\theta,\psi]$, $\boldsymbol{x}_2\in\mathbf{R}^{6\times1}=[u,v,w,p,q,r]$, $\boldsymbol{R}(\boldsymbol{\Theta})\in\mathbf{R}^{6\times6}$ is the rotation matrix, $\bar{\boldsymbol{M}}\in\mathbf{R}^{6\times6}$ is the airship mass matrix, $\bar{\boldsymbol{F}}_{\boldsymbol{D}}\in\mathbf{R}^{6\times1}$ is the dynamic force and dynamic torque vector. $\bar{\boldsymbol{F}}_{\mathrm{AS}}\in\mathbf{R}^{6\times1}$ is the aerostatic force and aerostatic torque vector. $\boldsymbol{F}_{\boldsymbol{W}}\in\mathbf{R}^{6\times1}$ is the vector of wind disturbance. $\bar{\boldsymbol{F}}_{\mathrm{AD}}\in\mathbf{R}^{6\times1}$ is the aerodynamic force and aerodynamic torque vector. $\boldsymbol{U}\in\mathbf{R}^{6\times1}$ is the generalized control force and control torque vector.

The description of the mass matrix is

$$\bar{\boldsymbol{M}}=\begin{bmatrix}m_x&0&0&0&m_{15}&0\\0&m_y&0&m_{24}&0&m_{26}\\0&0&m_z&0&m_{35}&0\\0&m_{42}&0&J_x&0&-J_{xz}\\m_{51}&0&m_{53}&0&J_y&0\\0&m_{52}&0&-J_{xz}&0&J_z\end{bmatrix}.\tag{2}$$

The mass matrix contains the airship actual mass and inertia as well as the added mass and inertia terms. The added terms come due to the mass of air displaced by the airship. Equation (3) gives a description of the dynamic force vector. The dynamic force vector summarizes the forces, torques acting on airship due to centrifugal, and Coriolis effects.

$$\bar{\boldsymbol{F}}_{\boldsymbol{D}}=\begin{bmatrix} -m_z wq+m_y rv+m\left[a_x\left(q^2+r^2\right)-a_z rp\right] \\ -m_x ur+m_z pw+m\left[-a_x pq-a_z rq\right] \\ -m_y vp+m_x qu+m\left[-a_x rp+a_z\left(q^2+p^2\right)\right] \\ -\left(J_z-J_y\right) rq+J_{xz} pq+ma_z(ur-pw) \\ -\left(J_x-J_z\right) pr+J_{xz}\left(r^2-p^2\right)+\cdots \\ m\left[a_x(vp-qu)-a_z(wq-rv)\right] \\ -\left(J_y-J_x\right) qp-J_{xz} qr+m\left[-a_x(ur-pw)\right] \end{bmatrix} \tag{3}$$

Equations (4) and (5) give the aerostatic and aerodynamic force vectors.

$$\bar{\boldsymbol{F}}_{\mathrm{AS}}=\begin{bmatrix} -(W-B_f)s_\theta \\ (W-B_f)c_\theta s_\phi \\ (W-B_f)c_\theta c_\phi \\ a_z W c_\theta s_\phi \\ -(a_z W-b_z B_f)s_\theta-(a_x W-b_x B_f)c_\theta c_\phi \\ a_x W c_\theta s_\phi \end{bmatrix} \tag{4}$$

where W is the airship weight, B_f is the buoyancy force, $\{a_x, a_z\}$ are the coordinates of the center of gravity (CG) of the airship with reference to the CV and $\{b_x, b_z\}$ are the coordinates of the center of buoyancy of the airship with reference to the CV. The notation $s_{(\cdot)}, c_{(\cdot)}, t_{(\cdot)}$ are used for $\sin(\cdot), \cos(\cdot)$ and $\tan(\cdot)$ respectively.

$$\bar{\boldsymbol{F}}_{\mathrm{AD}}=f(V_t)\begin{bmatrix} C_{X1}c_\alpha^2 c_\beta^2+C_{X2}s_{2\alpha}s_{\frac{\alpha}{2}} \\ C_{Y1}c_{\beta/2}s_{2\beta}+C_{Y2}s_{2\beta}+C_{Y3}s_\beta s_{|\beta|} \\ C_{z1}c_{\alpha/2}s_{2\alpha}+C_{z2}s_{2\alpha}+C_{z3}s_\alpha s_{|\alpha|} \\ C_{L2}s_\beta s_{|\beta|} \\ C_{M1}c_{\alpha/2}s_{2\alpha}+C_{M2}s_{2\alpha}+C_{M3}s_\alpha s_{|\alpha|} \\ C_{N1}c_{\beta/2}s_{2\beta}+C_{N2}s_{2\beta}+C_{N3}s_\beta s_{|\beta|} \end{bmatrix} \tag{5}$$

where $f(V_t)=1/2\rho V_t^2$, $V_t=\sqrt{(u^2+v^2+w^2)}$, α is angle of attack, $C_{ij}(i=X,Y,Z,L,M,N;j=1,2,3,4)$ is the aerodynamic coefficient.

Remark 1 Airship roll angle and pitch angle satisfy the bounds $\left\{|\phi|<\frac{\pi}{2};|\theta|<\frac{\pi}{2}\right\}$, which ensures the non-singularity of the rotation matrix.

Assumption 1 Airship CG point lies beneath the CV and its center of buoyancy is coincident with the CV. The airship is in a neutral buoyancy state such that its weight and buoyancy are equal. Consequently, the aerostatic forces do not affect the horizontal dynamics. The given 6-DOF equations ignore the aeroelastic effects and consider the airship as a rigid body. However, the controller design considers these effects as model uncertainties.

Assumption 2 Airship mass matrix terms, $m_x=m_{x0}+m_{x\Delta}$, $m_y=m_{y0}+m_{y\Delta}$, $m_z=m_{z0}+m_{z\Delta}$, $J_x=J_{x0}+J_{x\Delta}$, $J_y=J_{y0}+J_{y\Delta}$, $J_z=J_{z0}+J_{z\Delta}$, $J_{xz}=J_{xz0}+J_{xz\Delta}$, are uncertainty terms, where m_{x0}, m_{y0}, m_{z0}, J_{x0}, J_{y0}, J_{z0}, J_{xz0} are known part and $m_{x\Delta}$, $m_{y\Delta}$, $m_{z\Delta}$, $J_{x\Delta}$, $J_{y\Delta}$, $J_{z\Delta}$, $J_{xz\Delta}$, are unknown part. However, the unknown part is bounded by some upper bound, $\bar{m}_{x\Delta}$, $\bar{m}_{y\Delta}$, $\bar{m}_{z\Delta}$, $\bar{J}_{x\Delta}$, $\bar{J}_{y\Delta}$, $\bar{J}_{z\Delta}$, $\bar{J}_{xz\Delta}$, $\bar{m}_{ij\Delta}$. The aerodynamic model coefficient $C_{ij}=C_{ij0}+C_{ij\Delta}(i=X,Y,Z,L,M,N;j=1,2,3,4)$ are uncertain, where C_{ij0} is the known part and $C_{ij\Delta}$ is the unknown part. The unknown part is bounded by some upper bound $\bar{C}_{ij\Delta}$.

3. Controller design for trajectory tracking

Trajectory tracking control is the task of tracking a predefined time-varying reference path within a specific time. Let $\boldsymbol{x}_{1d}$, $\boldsymbol{x}_1$ represent the reference trajectory and actual trajectory, respectively, where $\boldsymbol{x}_{1d}=[x_d,y_d,z_d,\phi_d,\theta_d,\psi_d]$ and $\boldsymbol{x}_1=[x,y,z,\phi,\theta,\psi]$.

The trajectory tracking controller aims to bring the error equal to zero asymptotically, that is, $\boldsymbol{x}_e=\boldsymbol{x}_1-\boldsymbol{x}_{1d}$. Fig. 2 gives a visual representation of a trajectory-tracking problem.

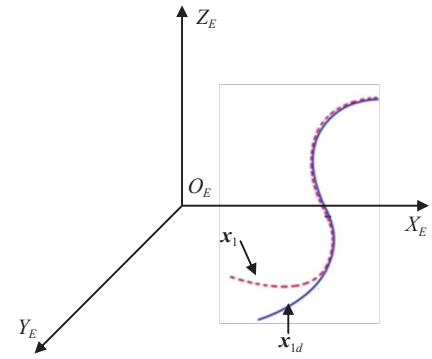

Fig. 2 Visual representation of a typical trajectory tracking problem

The equality formulation of the problem is as follows:

$$\lim_{t\to\infty}\boldsymbol{x}_e=\lim_{t\to\infty}|\boldsymbol{x}_1-\boldsymbol{x}_{1d}|=0. \tag{6}$$

Among the nonlinear controller options for the airship trajectory tracking, SMC is one of the simplest approaches. SMC is a variable structure control method. It alters the dynamics of the nonlinear system by applying a discontinuous control signal that forces the system to "slide" along the system's normal behavior [29]. SMC design can be broadly categorized into two parts. The first part deals with the designing of a sliding surface with desirable attributes like tracking and stability. The second part entails the designing of discontinuous control law that makes the sliding surface an invariant set. This control law also ensures that the sliding surface is a finite time reachable.

3.1 Model uncertainties representation using lumped approach

A lumped approach is introduced where a term $\Delta\boldsymbol{F}_{\mathrm{Mu}}$ in the airship model covers the model uncertainties. The modified model incorporating uncertainties is represented by

$$\begin{cases}\dot{\boldsymbol{x}}_1 = R(\boldsymbol{\Theta})\boldsymbol{x}_2 \\ \dot{\boldsymbol{x}}_2 = \boldsymbol{M}^{-1}(\boldsymbol{F}_{\boldsymbol{D}} + \boldsymbol{F}_{\mathrm{AS}} + \boldsymbol{F}_{\mathrm{AD}} + \boldsymbol{U}) + \Delta\boldsymbol{F}_{\mathrm{Mu}}\end{cases} \tag{7}$$

where

$$\Delta\boldsymbol{F}_{\mathrm{Mu}} = \bar{\boldsymbol{M}}^{-1}\left(\bar{\boldsymbol{F}}_{\boldsymbol{D}} + \bar{\boldsymbol{F}}_{\mathrm{AS}} + \bar{\boldsymbol{F}}_{\mathrm{AD}} + \boldsymbol{F}_{\boldsymbol{W}} + \boldsymbol{U}\right) - \boldsymbol{M}^{-1}(\boldsymbol{F}_{\boldsymbol{D}} + \boldsymbol{F}_{\mathrm{AS}} + \boldsymbol{F}_{\mathrm{AD}} + \boldsymbol{U}). \tag{8}$$

The terms $\boldsymbol{M}$, $\boldsymbol{F}_D$, $\boldsymbol{F}_{\mathrm{AS}}$ and $\boldsymbol{F}_{\mathrm{AD}}$ are defined in (2)–(5), respectively with nominal values as given in Assumption 2.

3.2 SMC design

The estimation error is defined as

$$\boldsymbol{x}_{\boldsymbol{e}} = \boldsymbol{x}_1 - \boldsymbol{x}_{1d}. \tag{9}$$

The error based linear hyperplane is defined as a sliding surface as follows:

$$\boldsymbol{S} = \dot{\boldsymbol{x}}_{\boldsymbol{e}} + \boldsymbol{a}\boldsymbol{x}_{\boldsymbol{e}} \tag{10}$$

with $\boldsymbol{a} = \mathrm{diag}(a_1, a_2, a_3, a_4, a_5, a_6)$. These terms are tuning variable and required to be positive to ensure the convergence of error to zero. After the design of the sliding surface, appropriate reaching law is chosen. The reaching law ensures that trajectories will converge to the sliding surface and will stay there. Here the simplest reaching law $-\boldsymbol{K}\tanh\boldsymbol{S}$ is adopted with hyperbolic tangent as a switching function. $\boldsymbol{K} = \mathrm{diag}(k_1, k_2, k_3, k_4, k_5, k_6)$ is the controller gain, which is positive and can be tuned heuristically; however, as for SMC the uncertain term $\Delta\boldsymbol{F}_{\mathrm{Mu}}$ is not available. For robustness to prevail, Assumption 3 should hold for SMC.

Assumption 3 It is assumed that there exists a positive number γ such that the uncertainty $\|\Delta\boldsymbol{F}_{\mathrm{Mu}}\| < \gamma$, and controller gain $\|\boldsymbol{K}\| > \gamma$.

For the trajectories to reach the sliding surface, the reachability condition should be satisfied, i.e., $\boldsymbol{S}\dot{\boldsymbol{S}} < 0$. For the validity of the condition, $\dot{\boldsymbol{S}}$ is selected as $-\boldsymbol{K}\mathrm{sign}(\boldsymbol{S})$, where $\mathrm{sign}(\cdot)$ is a signum function that is zero at $\boldsymbol{S} = 0$, one at $\boldsymbol{S} > 0$ and negative one at $\boldsymbol{S} < 0$.

Now, using (7) with the availability of bounds on $\Delta\boldsymbol{F}_{\mathrm{Mu}}$, as defined in Assumption 3 and reachability condition, the control law will be

$$\boldsymbol{U} = \boldsymbol{M}\boldsymbol{R}(\boldsymbol{\Theta})^{-1}\left(-\boldsymbol{K}\tanh\boldsymbol{S} - \dot{\boldsymbol{R}}(\boldsymbol{\Theta})\boldsymbol{x}_2 + \ddot{\boldsymbol{x}}_{1d} - \boldsymbol{a}\dot{\boldsymbol{x}}_{\boldsymbol{e}}\right) - (\boldsymbol{F}_{\boldsymbol{D}} + \boldsymbol{F}_{\mathrm{AD}} + \boldsymbol{F}_{\mathrm{AS}}). \tag{11}$$

Theorem 1 The airship model given in (7) with the sliding surface of (10) and control law given in (11), asymptotically stabilizes the closed-loop system.

Proof Select the Lyapunov function as follows:

$$\boldsymbol{V} = \frac{1}{2}\boldsymbol{S}^{\mathrm{T}}\boldsymbol{S} > 0. \tag{12}$$

Equation (13) is derived by differentiating (12) and expanding the terms.

$$\dot{\boldsymbol{V}} = \boldsymbol{S}^{\mathrm{T}}\dot{\boldsymbol{S}} = \boldsymbol{S}^{\mathrm{T}}[\ddot{\boldsymbol{x}}_{\boldsymbol{e}} + \boldsymbol{a}\dot{\boldsymbol{x}}_{\boldsymbol{e}}] \tag{13}$$

Equation (14) is derived by taking double derivative of (9).

$$\ddot{\boldsymbol{x}}_{\boldsymbol{e}} = \ddot{\boldsymbol{x}}_1 - \ddot{\boldsymbol{x}}_{1d} \tag{14}$$

Equation (15) is derived by using (7).

$$\ddot{\boldsymbol{x}}_{\boldsymbol{e}} = \dot{\boldsymbol{R}}(\boldsymbol{\Theta})\boldsymbol{x}_2 + \boldsymbol{R}(\boldsymbol{\Theta})\dot{\boldsymbol{x}}_2 - \ddot{\boldsymbol{x}}_{1d} = \dot{\boldsymbol{R}}(\boldsymbol{\Theta})\boldsymbol{x}_2 + \boldsymbol{R}(\boldsymbol{\Theta})\boldsymbol{M}^{-1}(\boldsymbol{F}_{\boldsymbol{D}} + \boldsymbol{F}_{\mathrm{AS}} + \boldsymbol{F}_{\mathrm{AD}} + \boldsymbol{U}) + \boldsymbol{R}(\boldsymbol{\Theta})\Delta\boldsymbol{F}_{\mathrm{Mu}} - \ddot{\boldsymbol{x}}_{1d} \tag{15}$$

Substitution of (15) into (13) gives

$$\dot{\boldsymbol{V}} = \boldsymbol{S}^{\mathrm{T}}[\dot{\boldsymbol{R}}(\boldsymbol{\Theta})\boldsymbol{x}_2 + \boldsymbol{R}(\boldsymbol{\Theta})\boldsymbol{M}^{-1}(\boldsymbol{F}_{\boldsymbol{D}} + \boldsymbol{F}_{\mathrm{AS}} + \boldsymbol{F}_{\mathrm{AD}} + \boldsymbol{U}) + \boldsymbol{R}(\boldsymbol{\Theta})\Delta\boldsymbol{F}_{\mathrm{Mu}} - \ddot{\boldsymbol{x}}_{1d} + \boldsymbol{a}\dot{\boldsymbol{x}}_{\boldsymbol{e}}]. \tag{16}$$

Substituting control law in (16) and simplifying:

$$\dot{\boldsymbol{V}} = -\boldsymbol{S}^{\mathrm{T}}[\boldsymbol{K}\tanh\boldsymbol{S} - \boldsymbol{R}(\boldsymbol{\Theta})\Delta\boldsymbol{F}_{\mathrm{Mu}}]. \tag{17}$$

Lyapunov condition is applicable for the inequality $\|\boldsymbol{K}\| > \gamma$.

$$\dot{\boldsymbol{V}} = -\boldsymbol{S}^{\mathrm{T}}[\boldsymbol{K}\tanh\boldsymbol{S} - \boldsymbol{R}(\boldsymbol{\Theta})\Delta\boldsymbol{F}_{\mathrm{Mu}}] < 0, \ \ S\,(t \neq 0). \tag{18}$$

□

Remark 2 The SMC controller given in (11) ensures the Lyapunov stability of the airship. The trajectory tracking error will asymptotically converge to zero within a finite time for the given bounds.

3.3 ESMC design for airship trajectory tracking

The bounds given in Assumption 3 undermines the performance of sliding mode controller. Estimation of model uncertainty and wind disturbance will ensure the performance of SMC beyond the given bounds. EKF is used to estimate the lumped model uncertainties and wind disturbance in the proposed algorithm.

Discussion: In the proposed ESMC method, EKF is designed to estimate the effect of model uncertainties and disturbances on the airship dynamics. It has been seen that for the airship trajectory tracking problem the conventional sliding mode controller performance is governed by the accurate model of the airship. In the presence of uncertainties and disturbances the conventional SMC performance deteriorates. However, If the controller is provided with a signal that encapsulates the lumping of model uncertainties and wind disturbance, then the performance of proposed ESMC is improved in term of robustness.

The discontinuous function in the SMC is the main source of chattering phenomena. In the proposed work, the signum function is replaced with tangent hyperbolic function along with the selection of small gains [29]. Moreover, the chattering reduces considerably, and the robustness increases if the controller is provided with lumped disturbance and model uncertainty information. This is because the gain can then be reduced, which results in improved performance with respect to chattering.

Fig. 3 shows the block diagram of the proposed ESMC. SMC is fed by reference trajectory and the estimate of airship states, model uncertainties and wind disturbance. The SMC calculates the control input and provides it to the airship system. In response to the control input, the airship tracks the desired trajectory effectively.

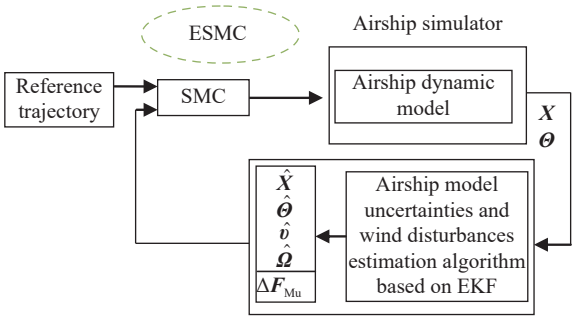

Fig. 3 Block diagram representation of proposed ESMC algorithm

Fig. 4 gives the flow chart of the proposed algorithm for efficient trajectory tracking of an airship.

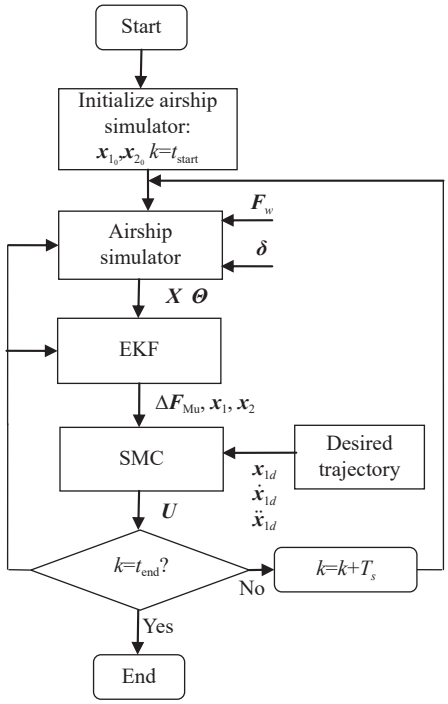

Fig. 4 Flow chart for the proposed airship trajectory tracking control algorithm

The airship simulator is initialized with initial values of position, attitude, linear, and angular velocities. Table 1 shows the possible initial values to be used in the airship simulator.

Table 1 Initial conditions for airship simulator

State	Symbol	Value
Position/m	$\boldsymbol{X}_0$	$[-20,400,80]$
Attitude/rad	$\boldsymbol{\Theta}_0$	$[0,0,0.484]$
Linear velocity/ms^{-1}	$\boldsymbol{v}_0$	$[5,0,0]$
Angular velocity/rads^{-1}	$\boldsymbol{\Omega}_0$	$[0,0,0]$

In the next step, the airship simulator receives control inputs, an information of wind disturbance and airship model parameter variations due to uncertainties. The estimates of position, and attitude from airship simulator are given to the EKF block [30]. EKF block implements the estimation algorithm that is based on the airship modified model given in (22) to estimate the airship state vector and model uncertainty vector. The EKF estimates the states and unknown parameters in the model on the bases of control input and sensor measurements. The information regarding states and unknown model parameters is given to SMC. The SMC block implements the proposed trajectory tracking control method. It utilizes the estimates of EKF and the desired trajectory and its derivative to calculate the control action. The stopping criteria of the algorithm depend on the total trajectory time and sampling rate, the relation for t_{end} can be given by

$$t_{\text{end}} = t_{\text{start}} + \frac{t_{\text{desired}}}{T_s} \tag{19}$$

where t_{desired} denotes the desired trajectory time, t_{start} denotes the start time of simulation experiment, T_s denotes the sampling time, and t_{end} denotes the end time of simulation experiment.

3.3.1 EKF design for airship model uncertainties and wind disturbance

EKF algorithm is a nonlinear extension of the famous Kalman filter. It gets the first-order linear approximation of the nonlinear system at each sampling time. For this sampling time, it acts as a linear Kalman filter. It is utilized widely in number of real-world applications for the estimation of unknown and un-measurable system states, unknown parameters, faults, and disturbances. For the application of the EKF algorithm, it is necessary to represent the nonlinear system in the state-space form. Moreover, additional state variables are introduced for the estimation of unknown parameters or disturbances.

In the proposed work, six augmented state variables are

introduced for the estimation of the airship model uncertainty vector $\Delta \boldsymbol{F}_{\mathrm{Mu}}$ as defined in a lumped approach. A system model given in (7) is modified for the application of the EKF algorithm.

Equation (20) introduces the augmented state vector.

$$\Delta \boldsymbol{F}_{\mathrm{Mu}} = \begin{bmatrix} \Delta F_u & \Delta F_v & \Delta F_w & \Delta F_p & \Delta F_q & \Delta F_r \end{bmatrix} \tag{20}$$

The compact representation for dynamic, aerodynamic, aerostatic, and control input vectors is given:

$$\boldsymbol{F} = \boldsymbol{F}_{\boldsymbol{D}} + \boldsymbol{F}_{\mathrm{AS}} + \boldsymbol{F}_{\mathrm{AD}} + \boldsymbol{U}. \tag{21}$$

Using (20), (21) and (7), airship modified nonlinear model in state-space form is represented by

$$\begin{bmatrix} \dot{\boldsymbol{x}}_1 \\ \dot{\boldsymbol{x}}_2 \\ \Delta \dot{\boldsymbol{F}}_{\mathrm{Mu}} \end{bmatrix} = \begin{bmatrix} \boldsymbol{R}(\boldsymbol{\Theta}) & \boldsymbol{O}_{6\times6} & \boldsymbol{O}_{6\times6} \\ \boldsymbol{O}_{6\times6} & \boldsymbol{M}^{-1} & \boldsymbol{I}_{6\times6} \\ \boldsymbol{O}_{6\times6} & \boldsymbol{O}_{6\times6} & \boldsymbol{O}_{6\times6} \end{bmatrix} \begin{bmatrix} \boldsymbol{x}_2 \\ \boldsymbol{F} \\ \Delta \boldsymbol{F}_{\mathrm{Mu}} \end{bmatrix}. \tag{22}$$

where $\boldsymbol{I}_{6\times6}$ represents an identity matrix and $\boldsymbol{O}_{6\times6}$ is a matrix having all zero elements. The modified airship model state vector consists of eighteen state elements, and it is defined by

$$\boldsymbol{X} = \begin{bmatrix} \boldsymbol{X} & \boldsymbol{\Theta} & \boldsymbol{\upsilon} & \boldsymbol{\Omega} & \Delta \boldsymbol{F}_{\mathrm{Mu}} \end{bmatrix}. \tag{23}$$

The state measurement vector can be defined by

$$\boldsymbol{Y} = \boldsymbol{C}\boldsymbol{X} = \begin{bmatrix} \boldsymbol{I}_{6\times6} & \boldsymbol{O}_{6\times12} \end{bmatrix} \boldsymbol{X}. \tag{24}$$

Equation (22) represents the continuous-time state-space representation of the airship model. Its compact representation is given by

$$\dot{\boldsymbol{X}} = f(\boldsymbol{X}, \boldsymbol{U}). \tag{25}$$

For the discrete-time EKF algorithm implementation, explicit first-order Euler integration is performed on (25). Moreover, it is augmented with process and measurement noise. The discrete-time representation of the model (25) is given by

$$\boldsymbol{X}_{k+1} = \boldsymbol{I}\boldsymbol{X}_k + \boldsymbol{T}_s f(\boldsymbol{X}_k, \boldsymbol{U}_k) + \boldsymbol{W}_p, \tag{26}$$

$$\boldsymbol{Y} = \boldsymbol{C}\boldsymbol{X} + \boldsymbol{W}_m, \tag{27}$$

where $\boldsymbol{X}_k$ represents the discrete-time state vector, $\boldsymbol{T}_s$ is the sampling time, $\boldsymbol{W}_p$ is the process noise vector, and $\boldsymbol{W}_m$ is the measurement noise vector.

EKF algorithm implementation is divided into two steps: prediction and correction. The process noise and measurement noise covariance matrixes are represented by $\boldsymbol{Q}$ and $\boldsymbol{R}$, respectively. $\boldsymbol{P}_k$ is the state error covariance matrix. The prediction and correction steps for each sampling instant are explained in the flowchart, as shown in Fig. 5. Prediction is divided into two steps: in the first step, states are predicted for the next sampling instant using the previous state estimates. In the second step, the state error covariance matrix is predicted for the next sampling instant using the model Jacobian matrix and process noise covariance matrix. Correction is accomplished using three steps. In the first step, Kalman filter gain $\boldsymbol{K}$ is calculated using the predicted state error covariance matrix. In the second step, states are corrected using available measurements and Kalman gain. In the third step, the prediction of the state error covariance matrix is made.

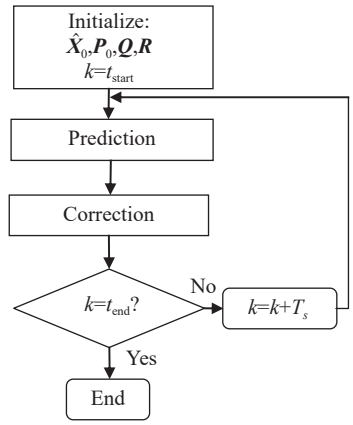

Fig. 5 Flow chart for the EKF algorithm

The prediction and correction steps use the following set of equations.

Prediction The prediction step is governed by

$$\tilde{\boldsymbol{X}}_{k+1} = f(\hat{\boldsymbol{X}}_k, \boldsymbol{U}_k), \tag{28}$$

$$\begin{cases} \tilde{\boldsymbol{P}}_{k+1} = \boldsymbol{\Phi}_k \hat{\boldsymbol{P}}_k \boldsymbol{\Phi}_k^{\mathrm{T}} + \boldsymbol{Q} \\ \boldsymbol{\Phi}_k = \dfrac{\partial f(\hat{\boldsymbol{X}}_k, \boldsymbol{U}_k)}{\partial \boldsymbol{X}_k}\Big|_{\hat{\boldsymbol{X}}_k} \end{cases}. \tag{29}$$

Correction The set of equations for the correction step are given as

$$\tilde{\boldsymbol{K}}_{k+1} = \tilde{\boldsymbol{P}}_{k+1} \boldsymbol{C}^{\mathrm{T}} (\boldsymbol{C} \tilde{\boldsymbol{P}}_{k+1} \boldsymbol{C}^{\mathrm{T}} + \boldsymbol{R})^{-1}, \tag{30}$$

$$\hat{\boldsymbol{X}}_{k+1} = \tilde{\boldsymbol{X}}_{k+1} + \tilde{\boldsymbol{K}}_{k+1} (\boldsymbol{Y} - \boldsymbol{C} \tilde{\boldsymbol{X}}_{k+1}), \tag{31}$$

$$\hat{\boldsymbol{P}}_{k+1} = (\boldsymbol{I} - \tilde{\boldsymbol{K}}_{k+1} \boldsymbol{C}) \tilde{\boldsymbol{P}}_{k+1}. \tag{32}$$

3.3.2 Controller formulation and stability analysis

Theorem 2 Using the estimate of $\Delta \boldsymbol{F}_{\mathrm{Mu}}$ provided by EKF that is based on (22) and airship nonlinear model incorporating model uncertainties defined in (1) and (7), the sliding surface defined in (10) and with the given reaching law the controller equation for ESMC will be

$$\boldsymbol{U} = \bar{\boldsymbol{M}} \boldsymbol{R}(\boldsymbol{\Theta})^{-1} \left(-\boldsymbol{K} \tanh \boldsymbol{S} - \dot{\boldsymbol{R}}(\boldsymbol{\Theta}) \boldsymbol{x}_2 + \ddot{\boldsymbol{x}}_{1d} - \boldsymbol{a} \dot{\boldsymbol{x}}_e \right) - (\bar{\boldsymbol{F}}_{\boldsymbol{D}} + \bar{\boldsymbol{F}}_{\mathrm{AS}} + \bar{\boldsymbol{F}}_{\mathrm{AD}} + \boldsymbol{F}_{\boldsymbol{W}}) \tag{33}$$

where $\bar{\boldsymbol{M}}$ is the mass matrix of airship with uncertain parameters.

Proof Using reaching law:

$$-\boldsymbol{K}\tanh\boldsymbol{S}=\dot{\boldsymbol{S}}=\ddot{\boldsymbol{x}}_e+\boldsymbol{a}\dot{\boldsymbol{x}}_e=\ddot{\boldsymbol{x}}_1-\ddot{\boldsymbol{x}}_{1d}+\boldsymbol{a}\dot{\boldsymbol{x}}_e=\dot{\boldsymbol{R}}(\boldsymbol{\Theta})\boldsymbol{x}_2+\boldsymbol{R}(\boldsymbol{\Theta})\dot{\boldsymbol{x}}_2-\ddot{\boldsymbol{x}}_{1d}+\boldsymbol{a}\dot{\boldsymbol{x}}_e=\dot{\boldsymbol{R}}(\boldsymbol{\Theta})\boldsymbol{x}_2+\boldsymbol{R}(\boldsymbol{\Theta})\boldsymbol{M}^{-1}(\boldsymbol{F}_D+\boldsymbol{F}_{\mathrm{AS}}+\boldsymbol{F}_{\mathrm{AD}}+\boldsymbol{U})+\boldsymbol{R}(\boldsymbol{\Theta})\Delta\boldsymbol{F}_{\mathrm{Mu}}-\ddot{\boldsymbol{x}}_{1d}+\boldsymbol{a}\dot{\boldsymbol{x}}_e. \tag{34}$$

Make substitution of $\Delta\boldsymbol{F}_{\mathrm{Mu}}$ from (8) in (34):

$$-\boldsymbol{K}\tanh\boldsymbol{S}=\dot{\boldsymbol{R}}(\boldsymbol{\Theta})\boldsymbol{x}_2+\boldsymbol{R}(\boldsymbol{\Theta})\boldsymbol{M}^{-1}(\boldsymbol{F}_D+\boldsymbol{F}_{\mathrm{AS}}+\boldsymbol{F}_{\mathrm{AD}}+\boldsymbol{U})+\boldsymbol{R}(\boldsymbol{\Theta})\bar{\boldsymbol{M}}^{-1}\left(\bar{\boldsymbol{F}}_D+\bar{\boldsymbol{F}}_{\mathrm{AS}}+\bar{\boldsymbol{F}}_{\mathrm{AD}}+\boldsymbol{F}_W+\boldsymbol{U}\right)-\boldsymbol{R}(\boldsymbol{\Theta})\boldsymbol{M}^{-1}(\boldsymbol{F}_D+\boldsymbol{F}_{\mathrm{AS}}+\boldsymbol{F}_{\mathrm{AD}}+\boldsymbol{U})-\ddot{\boldsymbol{x}}_{1d}+\boldsymbol{a}\dot{\boldsymbol{x}}_e. \tag{35}$$

Simplify (35) and there is

$$\boldsymbol{R}(\boldsymbol{\Theta})\bar{\boldsymbol{M}}^{-1}\boldsymbol{U}=-\boldsymbol{K}\tanh\boldsymbol{S}-\dot{\boldsymbol{R}}(\boldsymbol{\Theta})\boldsymbol{x}_2+\ddot{\boldsymbol{x}}_{1d}-\boldsymbol{a}\dot{\boldsymbol{x}}_e+\bar{\boldsymbol{M}}^{-1}\left(\bar{\boldsymbol{F}}_D+\bar{\boldsymbol{F}}_{\mathrm{AS}}+\bar{\boldsymbol{F}}_{\mathrm{AD}}+\boldsymbol{F}_W\right). \tag{36}$$

Equation (33) is obtained by separating control input from (36). □

Theorem 3 Using the airship model given in (1) and (7), the sliding surface defined in (10), the controller defined in (33), and the EKF estimator designed for estimating $\Delta\boldsymbol{F}_{\mathrm{Mu}}$ defined in (22) will stabilize the closed-loop system. The control law will perform the trajectory tracking task with trajectory tracking error asymptotically approaching zero.

Proof Select the Lyapunov function given in

$$\boldsymbol{V}=\frac{1}{2}\boldsymbol{S}^{\mathrm{T}}\boldsymbol{S}>0. \tag{37}$$

Differentiating (37) and expanding the terms can obtain that

$$\dot{\boldsymbol{V}}=\boldsymbol{S}^{\mathrm{T}}\dot{\boldsymbol{S}}=\boldsymbol{S}^{\mathrm{T}}[\ddot{\boldsymbol{x}}_e+\boldsymbol{a}\dot{\boldsymbol{x}}_e]. \tag{38}$$

Taking the time derivative of (9) twice we will get

$$\ddot{\boldsymbol{x}}_e=\ddot{\boldsymbol{x}}_1-\ddot{\boldsymbol{x}}_{1d}. \tag{39}$$

Using (7) and further simplifying (39), we can obtain that

$$\ddot{\boldsymbol{x}}_e=\dot{\boldsymbol{R}}(\boldsymbol{\Theta})\boldsymbol{x}_2+\boldsymbol{R}(\boldsymbol{\Theta})\dot{\boldsymbol{x}}_2-\ddot{\boldsymbol{x}}_{1d}=\dot{\boldsymbol{R}}(\boldsymbol{\Theta})\boldsymbol{x}_2+\boldsymbol{R}(\boldsymbol{\Theta})\boldsymbol{M}^{-1}(\boldsymbol{F}_D+\boldsymbol{F}_{\mathrm{AS}}+\boldsymbol{F}_{\mathrm{AD}}+\boldsymbol{U})+\boldsymbol{R}(\boldsymbol{\Theta})\Delta\boldsymbol{F}_{\mathrm{Mu}}-\ddot{\boldsymbol{x}}_{1d}. \tag{40}$$

Substitute (40) in (38), and obtain that

$$\dot{\boldsymbol{V}}=\boldsymbol{S}^{\mathrm{T}}[\dot{\boldsymbol{R}}(\boldsymbol{\Theta})\boldsymbol{x}_2+\boldsymbol{R}(\boldsymbol{\Theta})\boldsymbol{M}^{-1}(\boldsymbol{F}_D+\boldsymbol{F}_{\mathrm{AS}}+\boldsymbol{F}_{\mathrm{AD}}+\boldsymbol{U})+\boldsymbol{R}(\boldsymbol{\Theta})\Delta\boldsymbol{F}_{\mathrm{Mu}}-\ddot{\boldsymbol{x}}_{1d}+\boldsymbol{a}\dot{\boldsymbol{x}}_e]. \tag{41}$$

Using (8) and further simplifying (41), we can obtain that

$$\dot{\boldsymbol{V}}=\boldsymbol{S}^{\mathrm{T}}[\dot{\boldsymbol{R}}(\boldsymbol{\Theta})\boldsymbol{x}_2+\boldsymbol{R}(\boldsymbol{\Theta})\boldsymbol{M}^{-1}(\boldsymbol{F}_D+\boldsymbol{F}_{\mathrm{AS}}+\boldsymbol{F}_{\mathrm{AD}}+\boldsymbol{U})+\boldsymbol{R}(\boldsymbol{\Theta})\bar{\boldsymbol{M}}^{-1}\left(\bar{\boldsymbol{F}}_D+\bar{\boldsymbol{F}}_{\mathrm{AS}}+\bar{\boldsymbol{F}}_{\mathrm{AD}}+\boldsymbol{F}_W+\boldsymbol{U}\right)-\boldsymbol{R}(\boldsymbol{\Theta})\boldsymbol{M}^{-1}(\boldsymbol{F}_D+\boldsymbol{F}_{\mathrm{AS}}+\boldsymbol{F}_{\mathrm{AD}}+\boldsymbol{U})-\ddot{\boldsymbol{x}}_{1d}+\boldsymbol{a}\dot{\boldsymbol{x}}_e]. \tag{42}$$

Inserting the relation for control law from (38) into (42), we obtain that

$$\dot{\boldsymbol{V}}=\boldsymbol{S}^{\mathrm{T}}\left\{\dot{\boldsymbol{R}}(\boldsymbol{\Theta})\boldsymbol{x}_2+\boldsymbol{R}(\boldsymbol{\Theta})\bar{\boldsymbol{M}}^{-1}\left[\left(\bar{\boldsymbol{F}}_D+\bar{\boldsymbol{F}}_{\mathrm{AS}}+\bar{\boldsymbol{F}}_{\mathrm{AD}}+\boldsymbol{F}_W+\left(\bar{\boldsymbol{M}}\boldsymbol{R}(\boldsymbol{\Theta})\right)^{-1}\left(-\boldsymbol{K}\tanh\boldsymbol{S}-\dot{\boldsymbol{R}}(\boldsymbol{\Theta})\boldsymbol{x}_2+\ddot{\boldsymbol{x}}_{1d}-\boldsymbol{a}\dot{\boldsymbol{x}}_e\right)-\left(\bar{\boldsymbol{F}}_D+\bar{\boldsymbol{F}}_{\mathrm{AS}}+\bar{\boldsymbol{F}}_{\mathrm{AD}}+\boldsymbol{F}_W\right)\right)\right]-\ddot{\boldsymbol{x}}_{1d}+\boldsymbol{a}\dot{\boldsymbol{x}}_e\right\}, \tag{43}$$

$$\dot{\boldsymbol{V}}=\boldsymbol{S}^{\mathrm{T}}(-\boldsymbol{K}\tanh\boldsymbol{S})<0. \tag{44}$$

□

Remark 4 The ESMC controller designed in (33) ensures the Lyapunov stability of an airship system defined by (1). The controller ensures that the trajectory tracking error will asymptotically converge to zero within a finite time without satisfying Assumption 3.

In the proposed method, EKF makes an estimate of $\Delta\boldsymbol{F}_{\mathrm{Mu}}$ and provides that information to the SMC. The method ensures the closed-loop stability of the system without the constraint made in Assumption 3. The proposed method also mitigates the chattering issues that usually come due to the selection of large controller gains for robustness in the conventional SMC. The performance of the proposed trajectory tracking control scheme is evaluated using a nonlinear simulator designed for University of Engineering and Technology Taxila (UETT) airship.

4. Results and discussions

For the verification of controller performance, numerical simulations are performed using a variable step Runga-Kutta (R-K) method in Matlab/Simulink R2019b environment. The software is running on a computer having a CPU frequency of 2.5 GHz. The sampling time used for the simulation is 0.002 s. An experimental UETT airship 6-DOF nonlinear model is developed [31,32].

The initial conditions used for the airship simulator are given in Table 1 while the initial conditions used for EKF are given in Table 2 and Table 3.

Table 2 Initial conditions for EKF

State	Symbol	Value
Position/m	$\boldsymbol{X}_0$	$[-10,200,70]$
Attitude/rad	$\boldsymbol{\Theta}_0$	$[0,0,0]$
Linear velocity/ms^{-1}	$\boldsymbol{\upsilon}_0$	$[2,1,1]$
Angular velocity/rads^{-1}	$\boldsymbol{\Omega}_0$	$[0.2,0.3,0.1]$
Uncertainty vector	$\Delta\boldsymbol{F}_{\mathrm{Mu0}}$	$\begin{bmatrix}0&0&0&0&0&0\end{bmatrix}$

Table 3 Initial conditions for EKF

EKF parameter	Symbol	Value
Process noise covariance	$\boldsymbol{Q}$	diag(0.1, 0.1, 0.1, 0.1, 0.1, 0.1, 10, 10, 10, 10, 10, 10, 100, 100, 100, 100, 100, 100)
Measurement noise covariance	$\boldsymbol{R}$	diag(2, 2, 2, 2, 2, 2)
State error covariance	$\boldsymbol{P}_0$	diag(1, 1, 1, 1, 1, 1, 1, 1, 1, 1, 1, 1, 100, 100, 100, 100, 100, 100)

To increase the robustness of the conventional SMC method, high controller gains are selected given in Table 4. Since the ESMC algorithm provides the estimates for unknown parameters, the accurate model for the airship is available. As a result, the requirement for high gain to avoid chattering phenomena is vanished. The controller gains for the ESMC method are given in Table 5.

Table 4 Sliding mode controller gains

Controller parameter	Value
$\boldsymbol{a}$	diag(6, 6, 6, 6, 6, 6)
$\boldsymbol{K}$	diag(10, 10, 10, 10, 10, 10)

Table 5 EKF based sliding mode controller gains

Controller parameter	Value
$\boldsymbol{a}$	diag(2, 2, 2, 2, 2, 2)
$\boldsymbol{K}$	diag(6, 6, 6, 6, 6, 6)

Extensive simulations are performed where controller performance under mass matrix variations, aerodynamic parameter variations, and in the presence of wind disturbance are evaluated separately by considering three different cases. In each case, different trajectories are considered so that controller can be evaluated under different maneuver conditions.

4.1 Performance evaluation under airship mass matrix parameters variation

To check the robust performance of SMC and ESMC methods, mass matrix parameters like airship mass and inertia terms are changed during airship flight. This change is actually inevitable because, in a stratospheric airship, leakage of helium gas often causes the change in these parameters. The location of the CG also varies during the flight because the change in mass matrix parameters can affect the CG point. Robustness against the parameter variation for airship trajectory tracking control is validated through random change in all parameters. However, in most cases this variation is very small. In the proposed technique we have used 30% changes in mass matrix parameters. In this simulation case, wind disturbance is not considered. For the current case, the desired spiral reference trajectory is selected as follows:

$$\boldsymbol{X}_d = \begin{bmatrix} x_d \\ y_d \\ z_d \end{bmatrix} = \begin{bmatrix} 600\sin(0.01t) \\ 600\cos(0.01t) \\ -100-0.01t \end{bmatrix}. \tag{45}$$

Fig. 6 shows the trajectory tracking performance of SMC and ESMC methods. It shows that both controllers effectively track the trajectory from the starting point (−20, −400, 80) m to the endpoint (325, 380, 850) m. Fig. 7 shows the error convergence. The x-direct error decreases from 20 m to around zero within 10 s. The y-direct error decreases from 200 m to 1 m after 50 s and z-direct from 10 m to 0 m after 5 s. Results indicate that the proposed controller successfully track the desired trajectory and it also points out the asymptotic convergence of error in finite-time. The results agree with Theorem 1 and Theorem 3. It indicates that SMC stabilizes the close loop system if the model uncertainties obey the upper bound criteria. However, for SMC there are certain control errors.

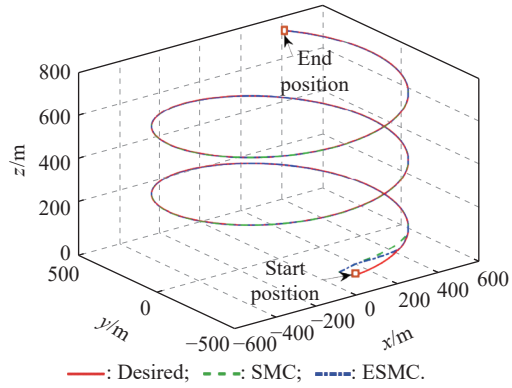

Fig. 6 Trajectory tracking performance of controllers

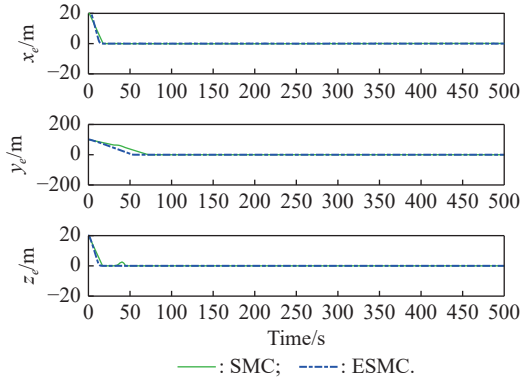

Fig. 7 Trajectory tracking error

Further, we can comment that the SMC method is robust against model uncertainties; however, SMC tackles model uncertainties with high-frequency control efforts. In the SMC method, once the controller has reached the sliding surface then its robustness benefits

can surely be obtained. However, these benefits are for those situations where uncertainties and disturbances do not exceed the specified bounds. We have applied the mass matrix variations after 100 s of simulation run when the controller already has reached the sliding surface. At the sliding surface, it handles the mass matrix variations with highly chattered control inputs, and it keeps the airship on the desired trajectory. However, if the model variations are applied before the controller reaches the sliding surface, then SMC convergence will also be affected. This fact is observed in Case 2 where controller performance is evaluated against aerodynamic model variations.

Fig. 8 shows the control efforts required for trajectory tracking. The figure shows the generalized forces and torques necessary for airship control. Fig. 8(i) shows the force required to accelerate the airship in the body axes forward direction. The initial magnitude of forward control force is small because the initial velocity of the airship is 5 ms^{-1}. It means that the airship is already in motion with a positive forward velocity that decreases the requirements of high control efforts to push the airship in a forward direction. The desired trajectory is spiral that requires constant control effort in the y-direction as well as constant control torque to maintain the airship roll angle. It also requires the torque for achieving the desired yaw rate.

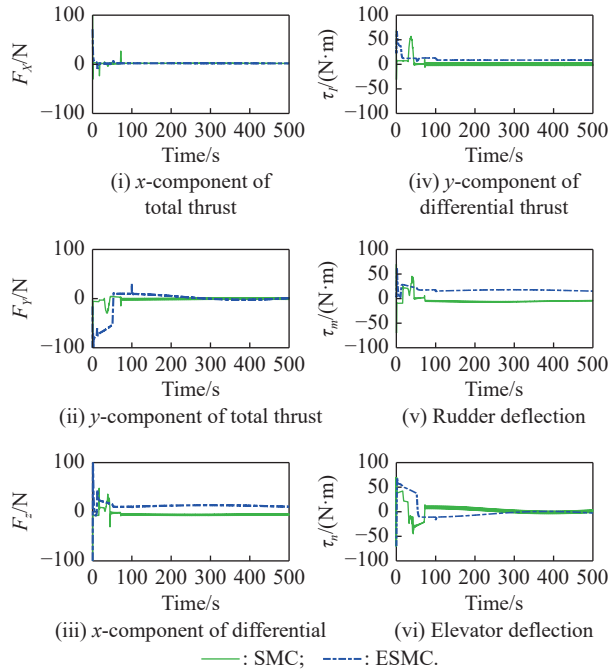

Fig. 8 Control effort

Fig. 8 (ii) shows the required y-directed force for achieving the desired side velocity. It indicates that initially, the force has a high magnitude however, after steady-state it maintains a constant positive magnitude necessary for tracking spiral trajectory. Fig. 8 (iv) shows the plot for roll torque. It generates the required roll rate. Fig. 8 (vi) shows the yaw torque. It maintains the desired yaw motion. Since the yaw angle is changing constantly so in steady-state yaw torque sticks to a positive value. The z directed component of force and pitch torque maintains a positive value because of the desired pitch angle. The control efforts calculated by ESMC are smooth as compared to the SMC method. The initial magnitudes for SMC are large as compared to the ESMC because SMC uses high gain for achieving robustness. Although SMC indicates the robust performance, however, it sacrifices the nominal performance. Fig. 9 shows the EKF estimations. Mass matrix parameters vary after 100 s that effect the body axes linear and angular accelerations. The effect of mass matrix variation is captured by the model uncertainty vector given by $\Delta \boldsymbol{F}_{\mathrm{MU}} = [\Delta F_u, \Delta F_v, \Delta F_w, \Delta F_p, \Delta F_q, \Delta F_r]\ g$.

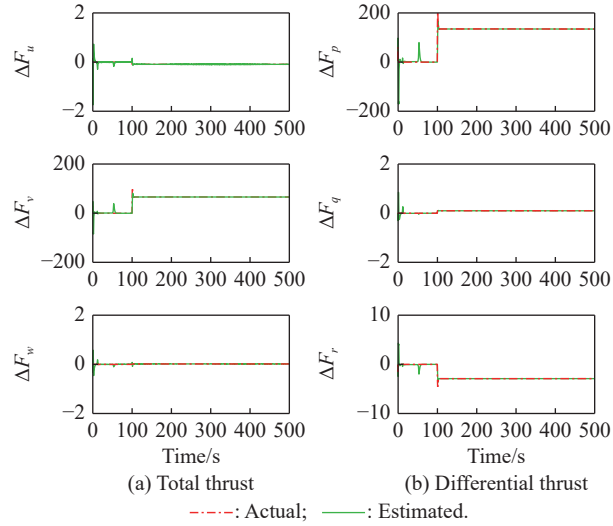

Fig. 9 Estimation of model uncertainties due to mass matrix parameter variations

4.2 Performance evaluation under variation of airship aerodynamic model

In this subsection, airship aerodynamic model inaccuracies are considered by introducing changes in aerodynamic forces and torques during airship cruise flight. We have used a 30% change in aerodynamic forces and torques. This subsection also considers the large initial biases in states. Generally, the accuracy of the initial values facilitates the convergence of the system. The best initial values give the best convergence. In our case, to give an allowance for inaccurate initial values we have tested our algorithm for a change of 20% in the accurate initial values. Further, the controller performance during

the reaching phase is tested. For this case, the controller tracks the desired straight-line 3D trajectory defined by

$$\boldsymbol{X}_d = \begin{bmatrix} x_d \\ y_d \\ z_d \end{bmatrix} = \begin{bmatrix} 2t \\ 2t \\ -100-0.5t \end{bmatrix}. \tag{46}$$

Fig. 10 shows the trajectory tracking performance of both controllers. It shows that ESMC successfully tracks the desired trajectory with the minimum tracking error from the starting position (−20, −400, 80) m to the end position (1 200, 1 200, 500) m while the SMC controller does not properly track the trajectory. Fig. 11 shows the tracking error in $x, y,$ and z directions for both controllers. It can be seen that the SMC method suffers from large errors, also its convergence is affected by model uncertainties. It is due to the fact that the SMC method has incomplete model information during the reaching phase.

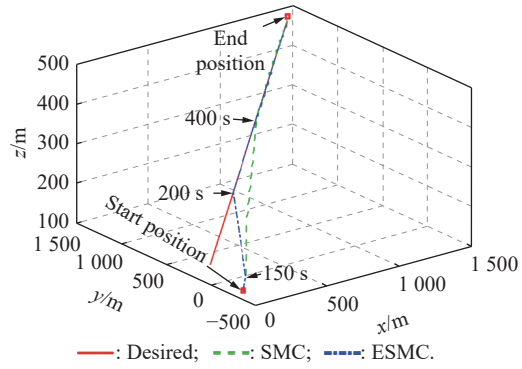

Fig. 10 Trajectory tracking performance of controllers

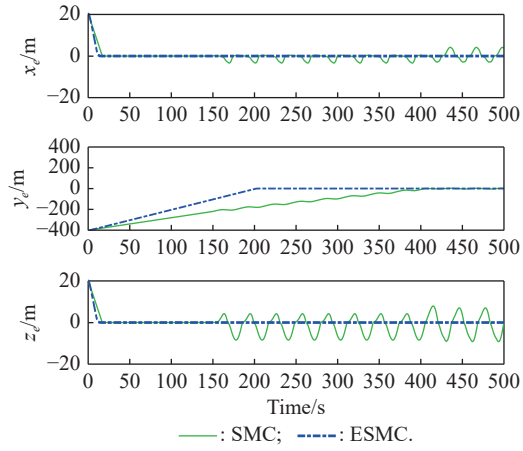

Fig. 11 Trajectory tracking error

At 150 s of a simulation run, aerodynamic model variations are applied. ESMC method converges to the sliding surface at 200 s while the SMC method takes 400 s. It indicates that incomplete model information during the reaching phase affects the SMC method, and it can lose its closed-loop stability while the ESMC method is invariant to the model uncertainties.

Fig. 12 shows the control efforts required for trajectory tracking. In this case, we have taken a straight-line 3D trajectory. The initial conditions of the airship simulator are away from the desired trajectory so a transient response can be seen between 0−200 s for the ESMC method. The trajectory tracking requires the airship to have some positive forward velocity, zero sway velocity, constant yaw angle, and a nose-up configuration. As the desired trajectory does not require the airship turning so the airship should have zero roll. Fig. 12 indicates that the control efforts fulfill the control requirements for the ESMC method. However, it can be seen that the SMC method suffers from chattering issues while the proposed method offers smooth control inputs that ensure the reliable performance.

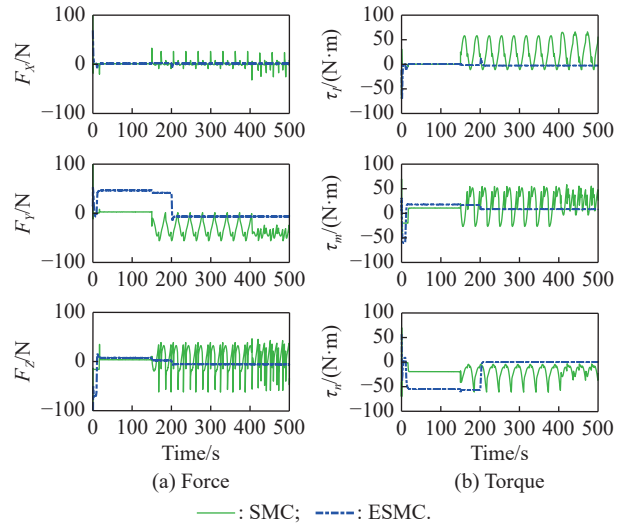

Fig. 12 Control effort

The estimation of changes in the aerodynamic model using EKF is shown in Fig. 13. It shows that EKF estimates the model uncertainty vector due to changes introduced in the aerodynamic model at 150 s. Our proposed algorithm has been tested for large initial biases and under aerodynamic model variation during the reaching phase of SMC. The results demonstrate that the proposed algorithm has improved convergence properties. It remains stable during the reaching phase and reaches the sliding phase after 200 s.

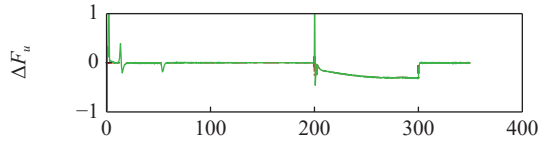

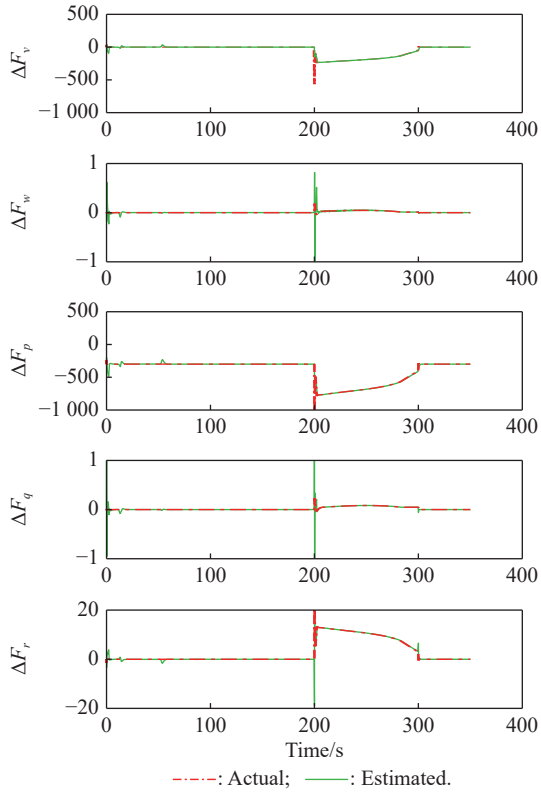

Fig. 13 Estimation of model uncertainties due to the change in aerodynamic model parameters

4.3 Wind disturbance case

In this subsection, controller performance under wind-disturbance is evaluated. The wind is an important factor that affects the flight performance of an airship. It is worthy to incorporate the effect of wind in controller design. In our approach, the disturbance due to the incident wind is explicitly estimated using EKF and it is integrated into the controller design. As it is intended to design a platform for observation applications like for surveillance and agricultural monitoring. Therefore, controller performance in low altitude environment is tested. The meteorological conditions of northern Pakistan show wind speed at 100 m of altitude is between 3 ms^{-1} and 6 ms^{-1} [33]. We have considered 5 m/s of wind speed. Apart from the constant wind, wind gust is also an important phenomenon usually occurring in northern Punjab because these landscapes are rough and they are surrounded by mountains. Wind gust is a brief increase in wind speed which usually lasts for 20 s. It has a transient characteristic and followed by a lull or slackening in the wind speed. Both wind gust and constant wind have been considered in the simulation. For the generation of wind gust, Dryden model power spectral density function is used to model the turbulent gust [34]. Gust velocities are generated by applying noise inputs having unitary power spectral density function to the following filters:

$$H_u(s)=\sqrt{\frac{2V_e\sigma_u^2}{L_u\pi}}\left[\frac{1}{s+\left(\frac{V_e}{L_u}\right)}\right], \tag{47}$$

$$H_v(s)=\sqrt{\frac{2V_e\sigma_v^2}{L_v\pi}}\left[\frac{s+\left(\frac{V_e}{\sqrt{3}L_u}\right)}{\left(s+\left(\frac{V_e}{L_v}\right)\right)^2}\right], \tag{48}$$

$$H_w(s)=\sqrt{\frac{2\sigma_w^2}{L_wV_e\pi}}\left[\frac{s+\left(\frac{V_e}{\sqrt{3}L_w}\right)}{\left(s+\left(\frac{V_e}{L_w}\right)\right)^2}\right]. \tag{49}$$

$\{L_u, L_v, L_w\}$ are the turbulence scale lengths that depend on air vehicle height. In simulation 100 m of altitude is considered so the turbulence scale lengths become $145h_t$, $145h_t$ and h_t where h_t=100 m, respectively. $\{\sigma_u, \sigma_v, \sigma_w\}$ are the intensities of turbulence in each direction. They are 0.5 ms^{-1}, 0.5 ms^{-1} and 0.042 ms^{-1}, respectively. The turbulence intensities depend on the wind speed on ground [35]. "s" is the Laplace operator and V_e is the equilibrium speed of the airship. The filters output the translational velocities $\{u_g, v_g, w_g\}$ of the atmospheric gusts. After 150 s of flight, the airship is subjected to 20 s of gust in x-y plane from 150 s to 170 s. The controller performance is also evaluated under the constant wind. The constant wind is directed from X_E-axis for 100 s between 200 s and 300 s of flight. The controller tracks the desired circular trajectory defined by

$$\boldsymbol{X}_d=\begin{bmatrix}x_d\\y_d\\z_d\end{bmatrix}=\begin{bmatrix}500\sin(0.01t)\\500\cos(0.01t)\\-100\end{bmatrix}. \tag{50}$$

Fig. 14 shows the trajectory tracking performance of both controllers. It can be seen that both controllers track the desired trajectory that starts from [0, −500, 100] m and ends at [0, −499, 100] m. Initially, the airship is at a location [−20, −400, −80] m. After 50 s of flight, it starts following the desired trajectory. The results indicate that the airship remains on the desired path during the course of complete flight under the command of ESMC. Fig. 15 shows the convergence of tracking error. It indicates that both controllers reach the error-based sliding surface after

50 s. The transient flight characteristics under both controllers are same because model uncertainties and wind disturbances in reaching phase are not considered. It is also observed that in the sliding phase ESMC remains on the surface during wind gust and steady wind speed. It indicates that the SMC method is robust against wind disturbances because it reaches the sliding surface before the wind disturbance occurs. However, the control inputs calculated by the SMC methos are affected by the chattering issue. The results agree with Theorem 2 which shows the SMC method's Lyapunov based stability and convergence with Assumption 3. However, if Assumption 3 is violated then SMC may diverge.

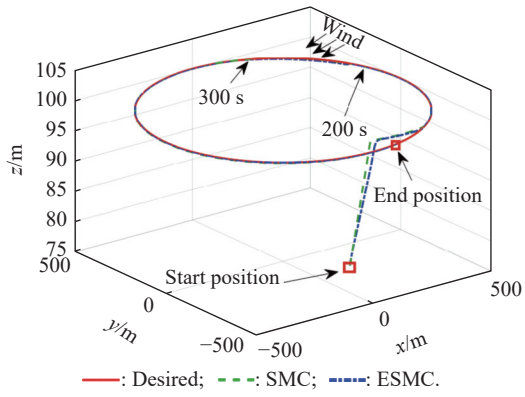

Fig. 14 Trajectory tracking performance of controllers

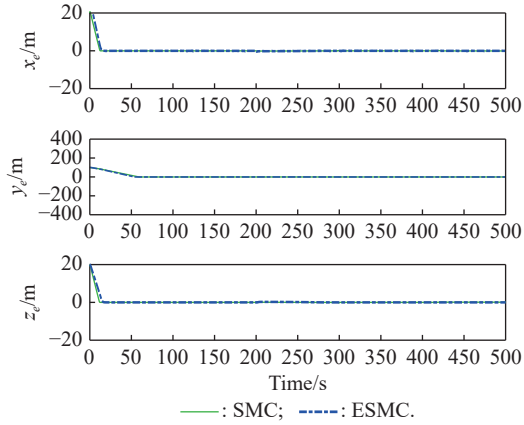

Fig. 15 Trajectory tracking error

The improvement in the results by the proposed method can be seen in Fig. 16 where control efforts are given. The results indicate that the control effort fulfills the control requirements. The ESMC method handles the wind disturbance efficiently as well as remains on the sliding surface. Moreover, it calculates smooth control input. Fig. 17 shows the estimation of the uncertainty vector due to wind forces by EKF.

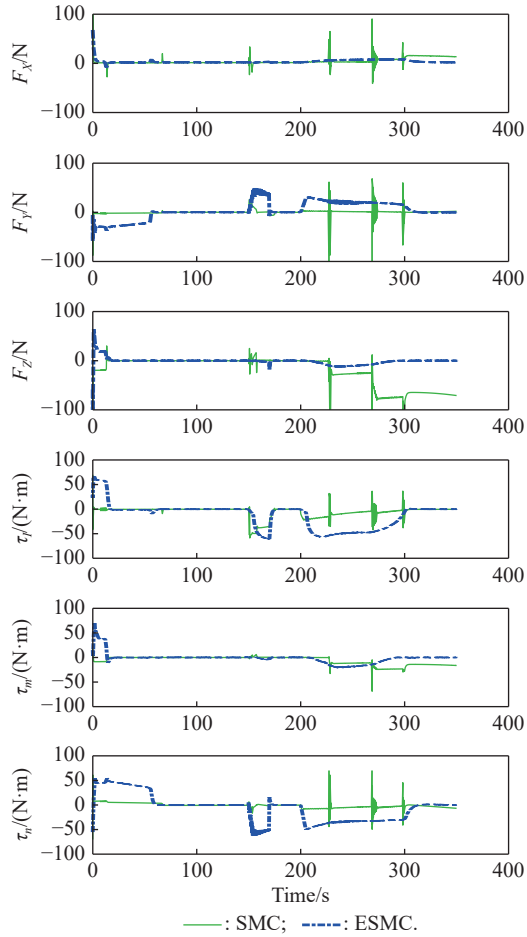

Fig. 16 Control effort

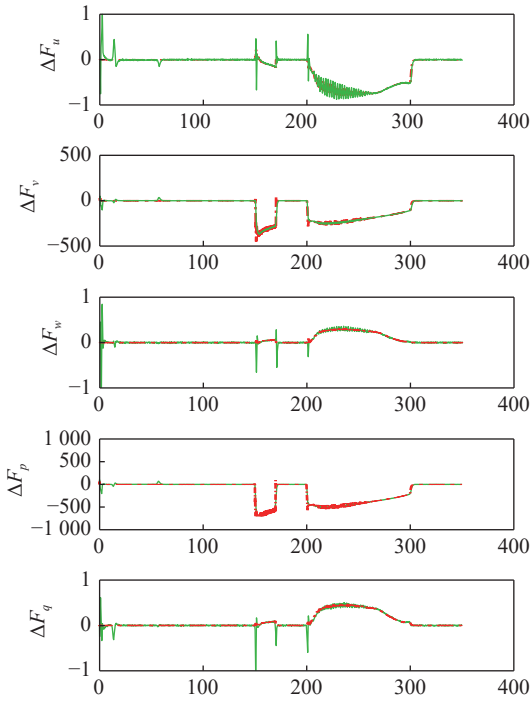

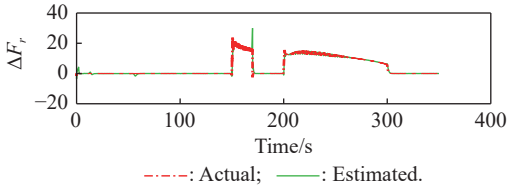

Fig. 17 Estimation of wind disturbances

The overall results show that EKF estimations aid the conventional SMC controller and improve its performance. The proposed ESMC method for trajectory tracking successfully tracks the desired trajectory in all cases. It calculates smooth control input as compared to SMC.

4.4 Performance analysis

The performance of the proposed algorithm for an airship trajectory tracking control problem is assessed by conducting a comparison analysis with the existing algorithms applied for the same problem. The existing control algorithms are divided in linear (PID), optimal (MPC, NMPC), nonlinear (gain scheduling, backstepping), and hybrid (adaptive backstepping, NN backstepping, adaptive SMC, adaptive integral SMC, fuzzy SMC, adaptive fuzzy SMC, NN-SMC, NN-NTSMC, and NN-fuzzy SMC) methods. The hybrid control methods exploit the benefits of adaptive, intelligent, and nonlinear algorithms to solve the airship trajectory tracking problem. In certain cases, the hybrid control methods result in a complex controller structure that often becomes difficult to realize. The controllers are discussed according to the following performance criteria [32]: (i) nominal system stability (NSS), (ii) robust system stability (RSS), (iii) dependence on accurate availability of states (DAAS), (iv) mass matrix variation (MMV), (v) aerodynamic model variation (AMV), (vi) wind disturbances (WD).

In Table 6, the performance of the proposed control method and the existing ones are summarized according to the above defined performance evaluation criteria. The columns correspond to the evaluation criteria while rows show the control method. The performance of the proposed method is summarized in the last row of the table. The entries for criteria NSS, RSS and DAAS are graded as Yes and No. Most of the existing methods for airship trajectory tracking control do not explicitly account for model uncertainties due to mass matrix variations and aerodynamic model variations. Therefore, the entries for MMV, AMV, and WD are graded as ‘considered’ and ‘not considered’.

Table 6 Performance evaluation and comparison of proposed method with existing method for airship trajectory tracking control problem

Technique	Reference	NSS	RSS	DAAS	MMV	AMV	WD
PID	[3]	Yes	No	Yes	Not considered	Not considered	Not considered
PID and dynamic inversion	[4,5]	Yes	No	Yes	Not considered	Not considered	Not considered
MPC	[6]	Yes	No	Yes	Not considered	Not considered	Considered
NMPC	[10]	Yes	No	Yes	Not considered	Not considered	Considered
Gain scheduling	[11]	Yes	Yes	Yes	Not considered	Not considered	Considered
BSC	[12]	Yes	No	Yes	Not considered	Not considered	Considered
Adaptive BSC	[13,14,15]	Yes	Yes	Yes	Not considered	Considered	Considered
NN-BSC	[16]	Mixed	Yes	Yes	Considered	Considered	Not considered
Adaptive SMC	[17,18]	Yes	Yes	Yes	Considered	Considered	Considered
Adaptive integral SMC	[19]	Yes	Yes	Yes	Considered	Considered	Considered
Fuzzy SMC	[20,21]	Mixed	Yes	Yes	Considered	Considered	Considered
Adaptive fuzzy SMC	[22]	Mixed	Yes	Yes	Considered	Considered	Considered
NN-SMC	[23]	Mixed	Yes	Yes	Considered	Considered	Considered
NN-NTSMC	[24,25]	Mixed	Yes	Yes	Considered	Considered	Considered
NN-Fuzzy-SMC	[26]	Mixed	Yes	Yes	Considered	Considered	Considered
ESMC	–	Yes	Yes	No	Considered	Considered	Considered

Table 6 shows that linear control methods guarantee the nominal system stability. They lack to ensure the robust system stability because there is no theoretical proof for linear controllers to establish the asymptotic stability of system. They are usually based on the linearized model of the system at certain operating conditions so they can only ensure the local stability. In hybrid method (PID plus dynamic inversion), although the operating range of system increases, the dynamic inversion control relies on the accurate plant information. In case of model uncertainties, it cannot ensure the robust system stability. PID controller has low implementation and computa-

tional complexity, so, it remains a first choice for industrial applications.

In optimal controllers, MPC and NMPC have been a choice among researchers. They can handle states and control input constraints. They ensure the nominal system stability, however do not guarantee the robust system stability. The MPC method solves an optimization problem on each sampling instant which makes them computationally intensive controllers and they are difficult to realize on hardware. That is why for airship trajectory tracking control they have not been much discussed. The existing papers about the MPC method for airship trajectory tracking control do not quote the results for assessing controller performance under criteria MMV and AMV.

In nonlinear controllers, BSC and gain scheduling controllers have been reported. The gain scheduling controller ensures both nominal and robust system stability. The BSC controller is designed based on the Lyapunov method and ensures the closed loop system stability. However, it requires the accurate system model information. It can ensure the RSS for certain bounds of uncertainties for which the controller is formulated. For reported gain scheduling and backstepping controller, authors have not considered the performance evaluation under airship parameter variations. To cope with the parameter variation issue, authors have suggested hybrid control methods. These methods are based on the idea of estimation of unknown parameters.

The reported hybrid controllers for the airship trajectory tracking problem combine the adaptive, intelligent, and nonlinear control methods. The study show that they ensure the robust system stability and good performance under criteria MMV, AMV, and WD. Although they exploit the benefits of different algorithms, but they pay the price in terms of high computational and implementational complexity. Apart from that, all existing algorithms explicitly assume the availability of all state estimates. However, in certain situations the states information can be lost due to sensor faults. In such situations, the model-based state estimator may do the job.

In the last row of the table the performance entries for the proposed algorithm are given. It exploits the benefits of both SMC and EKF. The EKF uses the model of airship and estimates the airship states, model uncertainties and wind disturbances. The method does not require an explicit state estimator. The proposed observer solves the problem of both state estimation and model uncertainties. The extensive simulation results evaluate its performance under mass matrix variations, aerodynamic model variations and wind disturbances. As a whole the ESMC method does not require the accurate state information. It can work under noisy measurements. It ensures both the nominal and robust stability because it does not rely on uncertainties bound. As compared to the hybrid methods, it has less computational complexity because all of the above stated methods explicitly require the state estimator, however, the proposed method extends the state estimation problem and combines it with unknown model parameters and external disturbance estimation.

5. Conclusions

EKF is used to provide accurate estimates for unknown model parameters. A hybrid control method for known and unknown model parameters couple with SMC enables airship to track desire trajectory with accuracy and perfection.

EKF based SMC improves robustness characteristics by designing a nonlinear estimation procedure for wind disturbances and airship model uncertainties. The proposed method convergence and stability analysis proves that the hybrid ESMC technique is closed-loop stable and convergent. Extensive simulations are performed for controller evaluation under the mass matrix parameter variations, aerodynamic forces and torque variations, and wind disturbances. The results show that the ESMC method is efficient and effective for steering the airship along the reference trajectory in finite-time. Further, the ESMC improves the robustness characteristics of the conventional SMC method and effectively alleviates the chattering issue.

From the information of hybrid sensor system, airship position, attitudes and known dynamic model parameters are estimated. These estimates warrant investigation of the effects induced by wind forces instead of measuring wind velocities by costly instrumentation.

The proposed method is easily realizable, cost effective and understandable. It allows variation in model parameters without compromising on the performance of airship trajectory tracking. As compared to the intelligent estimation solutions such as neural networks, the proposed method is a generic solution to the airship trajectory tracking control problem. It can be used for all types of UAV trajectory tracking control problems.

In the proposed work, airship is considered to be fully actuated, and the underactuated case can be considered as a future work.

References

[1] MILLER S H, FESEN R, HILLENBRAND L A, et al. Airships: a new horizon for science. Pasadena: The Keck Institute for Space Studies, 2014.

[2] GERKE M, MASAR I, BORGOLTE U, et al. Farmland monitoring by sensor networks and airships. Proc. of the 4th IFAC Conference on Modelling and Control in Agriculture,

2018: 321−326.
[3] DE PAIVA E C, BUENO S S, GOMES S B, et al. A control system development environment for AURORA's semiautonomous robotic airship. Proc. of the IEEE International Conference on Robotics and Automation, 1999: 2328−2335.
[4] CHEN L, ZHOU G, YAN X J, et al. Composite control of stratospheric airships with moving masses. Journal of Aircraft, 2012, 49(3): 794–801.
[5] MOUTINHO A, AZINHEIRA J R. Stability and robustness analysis of the aurora airship control system using dynamic inversion. Proc. of the IEEE International Conference on Robotics and Automation, 2005: 2265−2270.
[6] ZHANG J S, YANG X X, DENG X L, et al. Trajectory control method of stratospheric airships based on model predictive control in wind field. Proceedings of the Institution of Mechanical Engineers, Part G: Journal of Aerospace Engineering, 2019, 233(2): 418−25.
[7] WASIM M, KASHIF A S, ALI A, et al. Integrated AFS and DYC using predictive controller for vehicle handling improvement. Proc. of the IEEE 18th International Bhurban Conference on Applied Sciences and Technologies, 2021: 568−573.
[8] WASIM M, KASHIF A, AWAN A U, et al. Predictive control for improving vehicle handling and stability. Proc. of the IEEE International Conference on Intelligent Systems Engineering, 2016: 236−241.
[9] WASIM M, KASHIF A, AWAN A U, et al. H_∞ control via scenario optimization for handling and stabilizing vehicle using AFS control. Proc. of the IEEE International Conference on Computing, Electronic and Electrical Engineering, 2016: 307−312.
[10] YUAN J C, ZHU M, GUO X, et al. Trajectory tracking control for a stratospheric airship subject to constraints and unknown disturbances. IEEE Access, 2020, 8: 31453−31470.
[11] MOUTINHO A, AZINHEIRA J R, DE PAIVA E C, et al. Airship robust path-tracking: a tutorial on airship modelling and gain-scheduling control design. Control Engineering Practice, 2016, 50: 22−36.
[12] HAN D, WANG X L, CHEN L, et al. Command-filtered backstepping control for a multi-vectored thrust stratospheric airship. Transactions of the Institute of Measurement and Control, 2016, 38(1): 93–104.
[13] LIU S Q, GONG S J, LI Y X, et al. Vectorial backstepping method-based trajectory tracking control for an under-actuated stratospheric airship. The Aeronautical Journal, 2017, 121(1241): 916−939.
[14] HAN D, WANG X L, CHEN L, et al. Adaptive backstepping control for a multi-vectored thrust stratospheric airship with thrust saturation in wind. Proceedings of the Institution of Mechanical Engineers, Part G: Journal of Aerospace Engineering, 2016, 230(1): 45−59.
[15] LIU S Q, SANG Y J. Underactuated stratospheric airship trajectory control using an adaptive integral backstepping approach. Journal of Aircraft, 2018, 55(6): 2357−2371.
[16] YANG Y N, WANG W Q, YAN Y. Adaptive backstepping neural network control for three dimensions trajectory tracking of robotic airships. CEAS Aeronautical Journal, 2017, 8: 579−587.
[17] XIAO C, WANG Y Y, ZHOU P F, et al. Adaptive sliding mode stabilization and positioning control for a multi-vectored thrust airship with input saturation considered. Transactions of the Institute of Measurement and Control, 2018, 40(15): 4208−4219.
[18] ZHENG Z W, SUN L. Adaptive sliding mode trajectory tracking control of robotic airships with parametric uncertainty and wind disturbance. Journal of the Franklin Institute, 2018, 355(1): 106−122.
[19] XIAO C, HAN D, WANG Y Y, et al. Fault-tolerant tracking control for a multi-vectored thrust ellipsoidal airship using adaptive integral sliding mode approach. Proceedings of the Institution of Mechanical Engineers, Part G: Journal of Aerospace Engineering, 2018, 232(10): 1911−1924.
[20] YAO S Y, WANG H P, TIAN Y. Trajectory tracking control of a stratospheric airship with fuzzy sliding mode control. Proc. of the 37th IEEE Chinese Control Conference, 2018: 3955−3960.
[21] YANG Y N, YAN Y, ZHU Z L, et al. Positioning control for an unmanned airship using sliding mode control based on fuzzy approximation. Proceedings of the Institution of Mechanical Engineers, Part G: Journal of Aerospace Engineering, 2014, 228(14): 2627−2640.
[22] YANG Y N, WU J, ZHENG W. Trajectory tracking for an autonomous airship using fuzzy adaptive sliding mode control. Journal of Zhejiang University SCIENCE C, 2012, 13(7): 534−543.
[23] LOU W J, ZHU M, GUO X, et al. Command filtered sliding mode trajectory tracking control for unmanned airships based on RBFNN approximation. Advances in Space Research. 2019, 63(3): 1111−1121.
[24] YANG Y N, YAN Y. Neural network gain-scheduling sliding mode control for three-dimensional trajectory tracking of robotic airships. Proceedings of the Institution of Mechanical Engineers, Part I: Journal of Systems and Control Engineering. 2015, 229(6): 529−540.
[25] YANG Y N, YAN Y. Neural network approximation-based nonsingular terminal sliding mode control for trajectory tracking of robotic airships. Aerospace Science and Technology, 2016, 54: 192–197.
[26] YANG Y N, YAN Y. Trajectory tracking for robotic airships using sliding mode control based on neural network approximation and fuzzy gain scheduling. Proceedings of the Institution of Mechanical Engineers, Part I: Journal of Systems and Control Engineering, 2016, 230(2): 184−196.
[27] WASIM M, ALI A, CHOUDHRY M A, et al. Unscented Kalman filter for airship model uncertainties and wind disturbance estimation. PloS One. 2021, 16(11): e0257849.
[28] ASHRAF M Z, CHOUDHRY M A. Dynamic modeling of the airship with Matlab using geometrical aerodynamic parameters. Aerospace Science and Technology, 2013, 25(1): 56−64.
[29] LIU J. Sliding mode control using MATLAB. Beijing: Academic Press, 2017. (in Chinese)
[30] MathWorks. Sensor fusion and tracking Toolbox™: user's guide (R2019b). https://www.mathworks.com/help/pdf_doc/fusion/.
[31] WASIM M, ALI A. Estimation of airship aerodynamic forces and torques using extended Kalman filter. IEEE Access, 2020, 8: 70204–70215.

[32] WASIM M, ALI A. Airship aerodynamic model estimation using unscented Kalman filter. Journal of Systems Engineering and Electronics, 2020, 31(6): 1318−1329.
[33] Alliance for Sustainable Energy. Meteorological data of Pakistan. https://maps.nrel.gov/rede-pakistan/.
[34] VALLE R C, MENEGALDO L L, SIMOES A M. Smoothly gain-scheduled control of a tri-turbofan airship. Journal of Guidance, Control, and Dynamics, 2015, 38(1): 53−61.
[35] U.S. Department of Defense. Flying qualities of piloted aircraft, handbook MIL-HDBK-1797. Washington: U.S. Department of Defense, 1997.

Biographies

WASIM Muhammad was born in 1990. He received his M.S. degree in electrical engineering from Electrical and Mechanical Engineering College, National University of Sciences & Technology (NUST), Islamabad, Pakistan. He received his Ph.D. degree in electrical engineering with specialization of control system from University of Engineering and Technology Taxila, Taxila, Pakistan. He is currently working as an assistant professor at the Department of Aeronautics and Astronautics Engineering, Institute of Space Technology, Islamabad, Pakistan. His research interests include modelling and control of aerial vehicles, model uncertainty estimation using Kalman filter theory, nonlinear state observer, fault tolerant control, nonlinear control theory, construction of Lyapunov function for nonlinear systems, linear parameter-varying (LPV) modelling, and LPV control of airship.
E-mail: muhammad.077wasim@gmail.com

ALI Ahsan was born in 1977. He received his Ph.D. degree in control systems from TU Hamburg-Harburg, Germany. Currently, he is working as an associate professor with the Department of Electrical Engineering at University of Engineering and Technology Taxila, Pakistan. His research interests include machine learning, model identification, linear parameter-varying (LPV) modeling, and control design.
E-mail: ahsan.ali@uettaxila.edu.pk

CHOUDHRY Mohammad Ahmad was born in 1957. He received his B.S. degree in electrical engineering from University of Engineering and Technology Lahore, in 1982, M.S. from the George Washington University, USA in 1992 and Ph.D. degree from Virginia Tech, USA in 1995. He is a professor emeritus from the Department of Electrical Engineering, University of Engineering and Technology Taxila, Pakistan, where he worked as a full professor and the dean of the department. His research interests include renewable energy systems, power electronics, control system, and smart grids.
E-mail: dr.ahmad@uettaxila.edu.pk

SHAIKH Inam Ul Hasan was born in 1971. He received his Ph.D. degree in electrical engineering from University of Manchester, UK. Currently, he is working as an assistant professor with the Department of Electrical Engineering at University of Engineering and Technology Taxila, Pakistan. His research interests lie in iterative learning control, H_∞, nonlinear, and linear parameter-varying (LPV) control of the complex systems.
E-mail: inam.hassan@uettaxila.edu.pk

SALEEM Faisal was born in 1994. He is currently enrolled as a Ph.D. student at the Department of Measurements and Control Systems, the Joint Doctoral School, Silesian University of Technology, Gliwice, Poland. He received his B.S. degree in electrical engineering (EE) from University of Engineering and Technology (UET) Lahore in 2016 and M.S. degree in EE (control systems) from UET Taxila, Pakistan in 2018. From September 2019, he is also working as a lecturer in the department of EE at Riphah International University Islamabad, Pakistan. His research interests include evaluation of uncertainty of measurements, fractional-order (FO) modeling, and control design.
E-mail: faisal.saleem@polsl.pl